
Preliminary Extraction of DVCS Single- and Double-Spin Asymmetries on Polarized Nucleons with the CLAS12 Experiment

September 7, 2023

Noémie PILLEUX

IJCLab, Université Paris Saclay

Contents

1	Introduction	1
2	Dataset Used	4
3	Target Polarization Extraction	4
3.1	Measuring the Polarization	4
3.1.1	Theoretical Asymmetry	4
3.1.2	Event Selection	5
3.1.3	$P_b \times P_t$ Estimation	5
3.2	Dilution Factor	7
3.3	Results	8
4	DVCS analysis	10
4.1	Event Selection	10
4.2	Asymmetry Extraction	13
4.2.1	Dilution Factor	13
4.3	Asymmetries	13

Abstract

This is a report on the preliminary analysis of RGC data to extract beam-, target- and double-spin asymmetries for proton DVCS on an NH₃ target. An elastic analysis is first conducted to measure the target polarization. Preliminary DVCS asymmetries are then derived in ϕ bins at $\langle Q^2 \rangle = 2.5$, $\langle x_{bj} \rangle = 0.2$, $-t = 0.5$. These results are very preliminary as the dataset has yet to be fully calibrated. They do not provide a reliable measurement for the asymmetries but are rather shown as a demonstration of the potential of the RGC experiment and to prove that reasonable analysis tools are being developed. They will allow for measurements on ND_3 data, which is of particular interest to extract new observables, the target-spin and double-spin DVCS asymmetries for polarized neutrons and protons in deuterium.

1 Introduction

An intense research effort within the CLAS12 program at JLab is focused on the extraction of observables giving access to Generalized Parton Distributions (GPDs). GPDs give a three-dimensional picture of the partonic degrees of freedom of the nucleon in terms of longitudinal momentum, transverse spatial position, and their correlations. They are accessible in Deeply Virtual Compton Scattering (DVCS) experiments notably. At leading order and leading twist, and in CLAS12 kinematics, the DVCS process gives access to valence quarks in protons and neutrons. The leading diagram for DVCS is presented in Figure. 1.

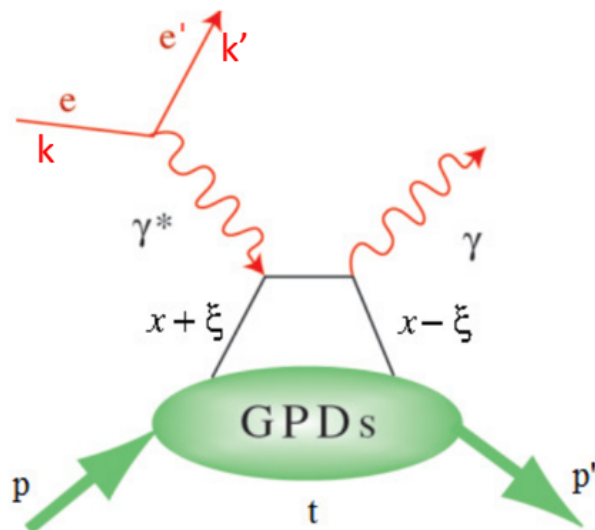


Figure 1: The DVCS process at leading order and leading twist. This diagram is based on QCD factorization. The incoming electron interacts via the exchange of a virtual photon with a single quark of the nucleon that propagates emitting a real photon. This is a QED interaction that is perturbative and calculable. The non-perturbative QCD processes describing the structure of the nucleon are encoded in GPDs. The diagram’s “hard” and “soft” parts are factorized to compute the amplitude.

The structure of the nucleon is described by four quark GPDs for each quark flavor q : $H_q, \tilde{H}_q, E_q, \tilde{E}_q$. They each describe different combinations of the beam helicity and of the relative orientation of the quark and nucleon spins. H and E do not depend on the quark helicity, contrary to \tilde{H} and \tilde{E} . H and \tilde{H} conserve the the nucleon spin while it is flipped with E and \tilde{E} .

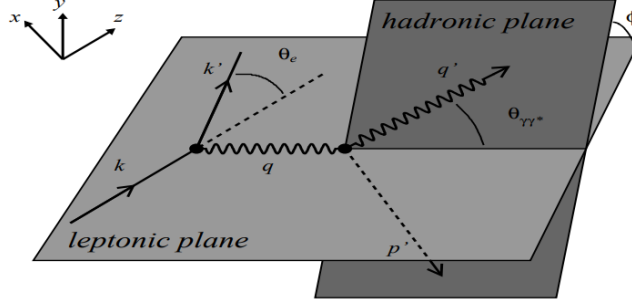


Figure 2: Definition of the ϕ angle between the leptonic plane (formed by the electrons and the virtual photon) and the hadronic plane (formed by the outgoing proton and real photon) in the $eN \rightarrow eN\gamma$ reaction.

The degrees of freedom encompassed in GPDs can be described by three variables. t is the squared four-momentum transfer between the initial and final nucleons. $x+\xi$ is the longitudinal momentum fraction carried by the struck quark before scattering and $x-\xi$ after scattering. In DVCS, x is integrated over, and we get access to Compton Form Factors (CFFs):

$$\mathcal{F}(\xi, t) = \int_{-1}^1 dx F(\mp x, \xi, t) \left[\frac{1}{x - \xi + i\epsilon} \pm \frac{1}{x + \xi - i\epsilon} \right] \quad (1)$$

where the top plus/minus sign refers to the unpolarized CFFs and the bottom one to their polarized counterparts. Hence, DVCS measurements combining polarized electron beams and polarized nucleon targets allow access to different CFFs. DVCS is indistinguishable from the Bethe-Heitler (BH) process in which the final state photon is not radiated by a quark of the nucleon but by the incoming or outgoing electron. The two processes interfere, and additional terms appear when computing the cross section from the process amplitudes and, therefore, in the asymmetries.

$$\mathcal{T} = |\mathcal{T}_{BH}|^2 + |\mathcal{T}_{DVCS}|^2 + \mathcal{I} \quad (2)$$

The decomposition into Fourier harmonics of each term with respect to the angle formed by the leptonic and hadronic planes (ϕ , defined in Fig.2) is the mathematical tool from which the CFFs can be extracted:

$$|\mathcal{T}_{BH}|^2 = \frac{e^6}{x_{bj}^2 y^2 (1 + \epsilon^2)^2 t \mathcal{P}_1(\phi) \mathcal{P}_2(\phi)} \left[c_0^{BH} + \sum_{n=1}^2 c_n^{BH} \cos(n\phi) + s_1^{BH} \sin(\phi) \right] \quad (3)$$

$$|\mathcal{T}_{DVCS}|^2 = \frac{e^6}{y^2 Q^2} \left[c_0^{DVCS} + \sum_{n=1}^2 c_n^{DVCS} \cos(n\phi) + s_n^{DVCS} \sin(n\phi) \right] \quad (4)$$

$$\mathcal{I} = \frac{e^6}{x_{bj} y^3 t \mathcal{P}_1(\phi) \mathcal{P}_2(\phi)} \left[c_0^{\mathcal{I}} + \sum_{n=1}^3 c_n^{\mathcal{I}} \cos(n\phi) + s_n^{\mathcal{I}} \sin(n\phi) \right] \quad (5)$$

In the BH term (3), \mathcal{P}_1 and \mathcal{P}_2 are the lepton propagators appearing in the BH amplitude, and the Fourier coefficients depend on the nucleon Form Factors (FFs) and are precisely calculable in QED. In the DVCS and interference terms (4),(5), the Fourier coefficients depend on the CFFs.

The single- and double-spin asymmetries can then be computed from the cross sections. At twist-two level,

$$A_{LU}(\phi) \simeq \frac{s_{1,unp}^I \sin(\phi)}{c_{0,unp}^{BH} + (c_{1,unp}^{BH} + c_{1,unp}^I + \dots) \cos(\phi) + \dots}$$

$$\text{with } s_{1,unp} \propto \Im \left[F_1 \mathcal{H} + \xi(F_1 + F_2) \tilde{\mathcal{H}} - \xi \frac{t}{4M^2} F_2 \mathcal{E} \right]. \quad (6)$$

The interference with the BH term is convenient, as shown in this equation: the $s_{1,unp}$ term is a linear combination of the imaginary part of four CFFs, and no quadratic terms appear.

$$A_{UL}(\phi) \simeq \frac{s_{1,LP}^I \sin(\phi)}{c_{0,unp}^{BH} + (c_{1,unp}^{BH} + c_{1,unp}^I + \dots) \cos(\phi) + \dots}$$

$$\text{with } s_{1,LP} \propto \Im \left[F_1 \tilde{\mathcal{H}} + \xi(F_1 + F_2) \left(\mathcal{H} + \frac{x_{bj}}{2} \mathcal{E} \right) - \xi \left(\frac{x_{bj}}{2} F_1 + \frac{t}{4M^2} F_2 \right) \tilde{\mathcal{E}} \right] \quad (7)$$

F_1 and F_2 are the Dirac and Pauli FFs. For the proton, the dominant terms are $\Im \tilde{H}_p$ and $\Im H_p$. For the neutron, $F_2 \gg F_1$ and the dominant term is $\Im H_n$.

$$A_{LL}(\phi) \simeq \frac{c_{0,LP}^{BH} + c_{0,LP}^I + (c_{1,LP}^{BH} + c_{1,LP}^I) \cos(\phi)}{c_{0,unp}^{BH} + (c_{1,unp}^{BH} + c_{1,unp}^I + \dots) \cos(\phi) + \dots}$$

$$\text{with } c_{0,LP}^I, c_{1,LP}^I \propto \Re \left[F_1 \tilde{\mathcal{H}} + \xi(F_1 + F_2) \left(\mathcal{H} + \frac{x_{bj}}{2} \mathcal{E} \right) - \xi \left(\frac{x_{bj}}{2} F_1 + \frac{t}{4M^2} F_2 \right) \tilde{\mathcal{E}} \right] \quad (8)$$

The constant and $\cos(\phi)$ terms contain both BH and interference contributions. It is expected to be sensitive to $\Re \tilde{\mathcal{H}}_p$ and $\Re \tilde{\mathcal{H}}_n$ mostly.

Therefore, measuring DVCS asymmetries gives a path to the extraction of CFFs. Combining polarized protons and neutrons with polarized electron beams allows access to different kinds of CFFs. They in turn give access to GPDs and to a three-dimensional description of the nucleon, to the origin of its spin, and to the forces at play within it. Moreover, measuring DVCS on both protons and neutrons is crucial to get a flavor-decomposition of GPDs. Indeed,

$$\mathcal{F}_p(\xi, t) = \frac{4}{9} \mathcal{F}_u(\xi, t) + \frac{1}{9} \mathcal{F}_d(\xi, t) \quad (9)$$

$$\mathcal{F}_n(\xi, t) = \frac{4}{9} \mathcal{F}_d(\xi, t) + \frac{1}{9} \mathcal{F}_u(\xi, t) \quad (10)$$

Combining equations 9 and 10, the quark GPDs can be extracted separately for u and d quarks.

All these efforts to measure unpolarized and polarized DVCS on both protons and neutrons are encompassed in the CLAS and CLAS12 physics programs. The CLAS12 RGB experiment is allowing for measurement of the beam-spin asymmetry on unpolarized protons and neutrons, which is of particular interest to extract the neutron GPD E_n . Target-spin and double-spin asymmetries on polarized protons in H have been performed at 6 GeV with the CLAS experiment. The RGC experiment will extend this program by measuring two new observables, namely the target-spin and double-spin asymmetries to polarized protons and neutrons in deuterium.

2 Dataset Used

These preliminary results have been processed using RGC runs:

- Positively polarized NH₃ data (NH_3+): 16317, 16318, 16320, 16321, 16322, 16323, 16325, 16327, 16328, 16329, 16330, 16331, 16332, 16333.
- Negatively polarized NH₃ data (NH_3-): 16335, 16336, 16337, 16338, 16339, 16341, 16343, 16345, 16346, 16348, 16350, 16352, 16353, 16354, 16355, 16356, 16357.
- Carbon data: 16291, 16293, 16296, 16297

They were cooked on the 30th of April 2023 with COATJAVA 8.7.0 (before the official "pass2" release). They were chosen, based upon the calibration timelines done in those days, to be roughly within the QA specifications for the main subdetectors. However, they do not include refined calibrations and have not been aligned, which shows in variables correlating information between the FD and the CD in particular (Section 3.1.2). This sample represents 21% of the NH_3 data taken in the summer 2022 period of RGC, using the Forward Tagger, and 31% of the C data from the same period.

3 Target Polarization Extraction

3.1 Measuring the Polarization

The beam polarization P_b and target polarization P_t need to be taken into account to correct the asymmetries measured from raw count rates. The beam polarization is monitored regularly during data taking with a Moller Polarimeter. While the experiment is running, Nuclear Magnetic Resonance (NMR) is used to monitor the target polarization but cannot give an absolute measurement of the target polarization. The NMR coils being placed on the surface of the target, the information they provide is mainly sensitive to its outer layers. The central part of the target is mostly exposed to the beam and depolarizes more rapidly, so surface information is insufficient for a reliable extraction of P_t .

A reliable method to extract the true $P_b \times P_t$ product comes from data analysis of quasi-elastic events. The theoretical asymmetry for quasi-elastic events (A_{th}) is well determined for the proton since the ratio of its electric and magnetic form factors has been measured precisely. The idea is then to extract $P_b \times P_t$ from the ratio of the measured asymmetry A_{meas} and A_{th} : $P_b P_t = \frac{A_{meas}}{A_{th}}$.

Therefore, the asymmetry is measured using (quasi-)elastic scattering in the NH_3 and ND_3 targets, accounting for the N background by estimating the dilution factor f that corresponds to the fraction of polarized nucleons inside the target. It is then compared to the theoretical prediction. This procedure is done in Q^2 bins, as explained in Sec. 3.1.3.

3.1.1 Theoretical Asymmetry

The elastic double-spin asymmetry A_{\parallel} from the proton can be computed using the electromagnetic form factors $G_E(Q^2)$ and $G_M(Q^2)$, and their ratio $G = \frac{G_M}{G_E}$.

$$A_{\parallel} = \frac{2\tau G[\frac{M}{E} + G(\tau \frac{M}{E} + (1 + \tau) \tan(\frac{\theta}{2})^2)]}{1 + G^2 \frac{\tau}{\epsilon}} \quad (11)$$

where E is the beam energy, M the proton mass, θ the polar angle of the scattered electron, $\tau = \frac{Q^2}{4M^2}$, $\epsilon = \frac{1}{1+2(1+\tau)\tan(\theta/2)^2}$.

The theoretical asymmetry is computed in Q^2 bins according to [1].

3.1.2 Event Selection

Quasi-elastic events are extracted from the exclusive measurement $ep \rightarrow ep$. The standard particle identification from the CLAS12 Event-Builder reconstruction algorithm is used. Data from the “gmn” trains are processed, pre-selecting events with at least one electron with $Q^2 > 0.95$ and $W < 2$. Events with exactly one electron and one proton are then selected. This choice was made for simplicity since selecting events with more than one proton or electron increases the statistics by less than 5% after applying the exclusivity cuts described below. Only particles with $|\chi_{pid}^2| < 3$ are kept.

Kinematics and exclusivity variables are computed from the reconstructed position and momenta of the protons and electrons. The virtual photon 4-vector (q) is constructed as the difference between the beam and detected electron 4-vectors. It is then possible to construct $W^2 = (p_p + q)^2$ using the proton 4-vector (p_p). The coplanarity $\Delta\phi = \phi_{e^-} - \phi_p$ is computed as the difference between the azimuthal angles of the detected proton and electron. The beam energy is estimated from the proton and electron polar angles, $E_{beam}^{calc} = M(\frac{1}{\tan(\theta_{e^-}/2)\tan(\theta_p)} - 1)$. The missing mass squared of the reaction is computed from the 4-vectors of the initial electron (p_{beam}), initial proton (p_{target}) and final electron (p_{e^-}) and proton (p_p) as $mm_{ep \rightarrow ep}^2 = (p_{beam} + p_{target} - p_{e^-} - p_p)^2$.

The W^2 , $\Delta\phi$, $mm_{ep \rightarrow ep}^2$, and E_{beam}^{calc} distributions are then fitted with Gaussian functions, and cuts are defined as 3σ cuts around the mean of each.

Fig. 3 shows the exclusivity cuts derived for the elastic events using protons detected in the CD or FD. The exclusivity cuts are relatively loose to preserve statistics. The δP_{e^-} and δP_p variables are the difference between the reconstructed momenta of the electron and proton and the momenta computed from elastic kinematics. Carbon and NH_3 data are compared: H events detach clearly as peaks above the N background, whose distributions are similar to the C data. For CD protons (Fig.3b), the coplanarity shows a double peak around the expected $\pm 180^\circ$, which is due to misalignment between the CD (where the proton angle is measured) and FD (where the electron angle is measured) information.

3.1.3 $P_b \times P_t$ Estimation

$P_b \times P_t$ is extracted using maximum likelihood estimation.

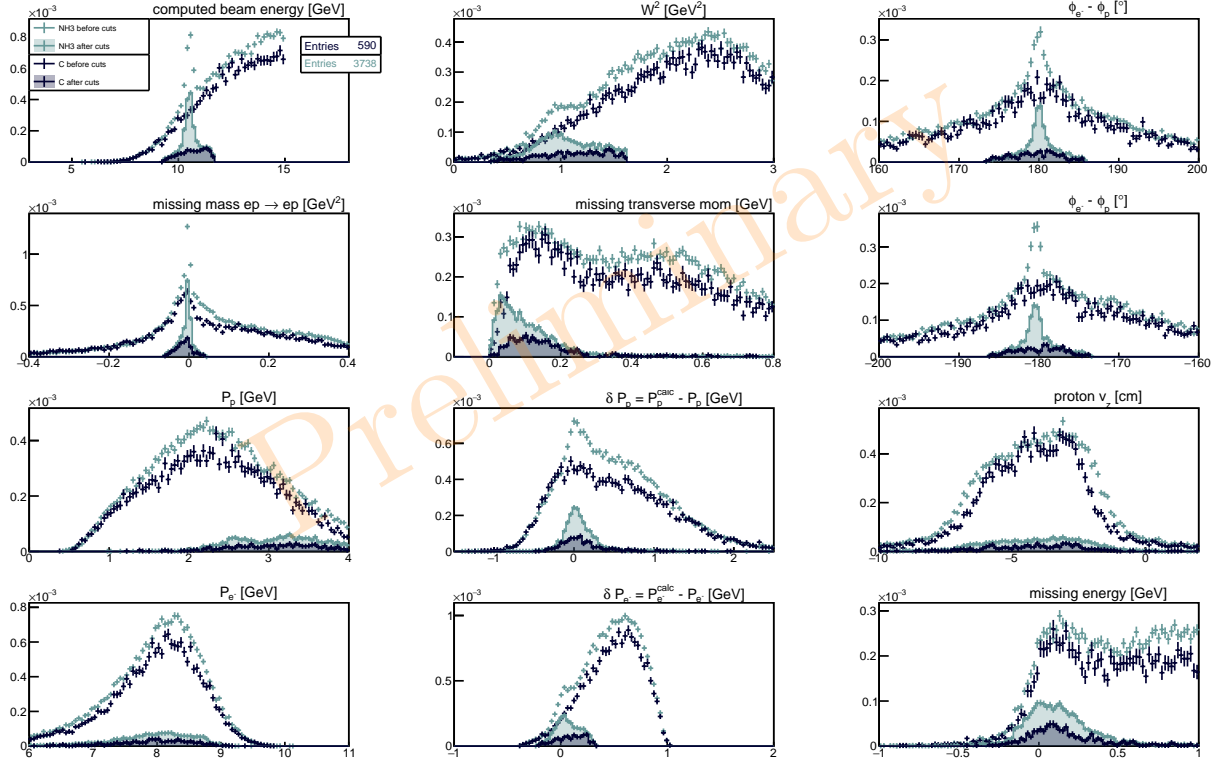
Let us note e_i the probability of having any event in a Q^2 bin labeled i , p_i^\pm the probability of having an event with helicity \pm in that bin and A_i the asymmetry in that bin.

$$\begin{cases} e_i = p_i^+ + p_i^- \\ A_i = \frac{p_i^+ - p_i^-}{e_i} \end{cases} \rightarrow p_i^\pm = \frac{e_i}{2}(1 \pm A_i) \quad (12)$$

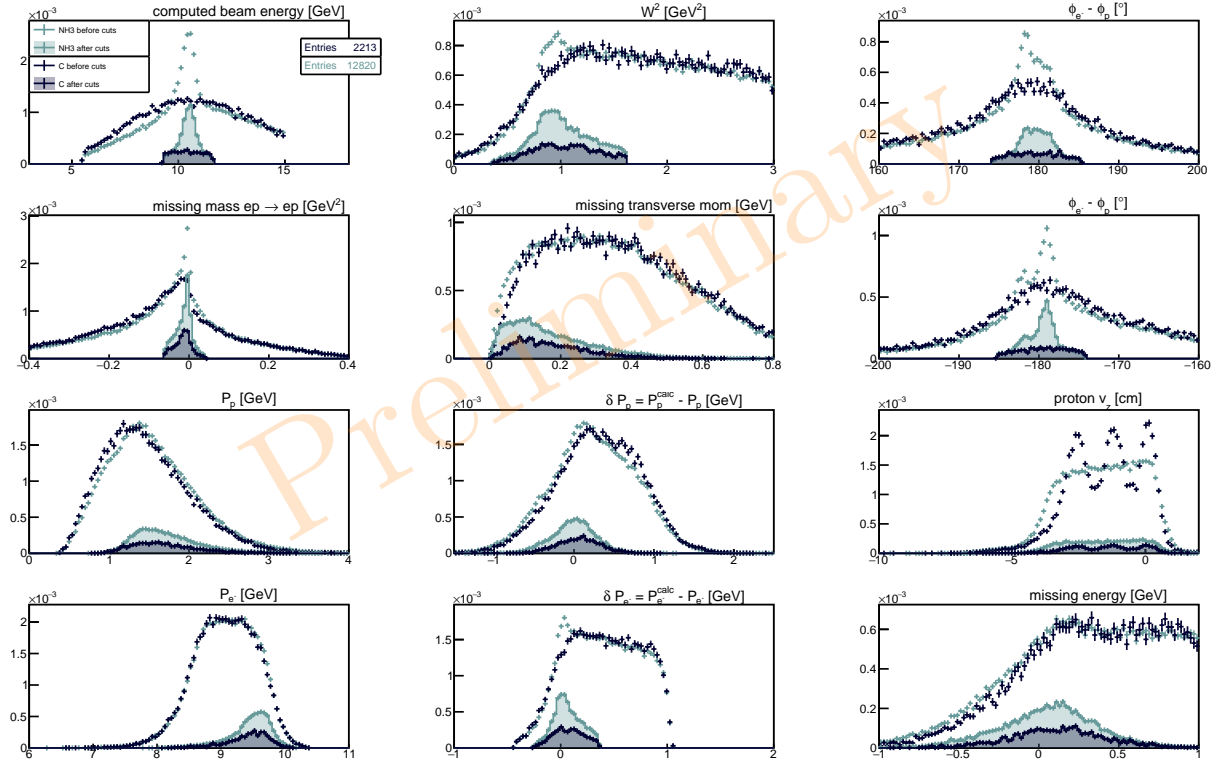
The probability to have N_i^\pm with helicity \pm in bin i is now given by:

$$p_{N_i^\pm}^\pm = \frac{(p_i^\pm)^{N_i^\pm} e^{-p_i^\pm}}{N_i^\pm!} \quad (13)$$

The likelihood function giving the probability to have N_i^\pm events with helicity \pm in every bin is given by:



(a) FD protons



(b) CD protons

Figure 3: Elastic exclusivity variables for NH_3 (in green) and C (in black) data. The comparison before (simple points) and after (filled distribution) cuts highlights the selection of the H peak above the N background. The first row shows distributions for the beam energy computed from the electron and proton kinematics, for W^2 , and for the coplanarity. The second row shows missing masses of the system. The third and fourth rows show the proton and electron kinematics, respectively.

$$L = \prod_{i=0}^{N_{bins}} p_{N_i^+} p_{N_i^-} \quad (14)$$

We try and maximize $l = \ln(L)$ with respect to $P = \frac{A_i}{f_i A_{th,i}}$ to find a good estimator for $P = P_t \times P_b$. f_i is the dilution factor in bin i and $A_{th,i}$ the theoretical asymmetry in that bin.

$$\frac{dl}{dP} = 0 \leftrightarrow \sum_{i=0}^{N_{bins}} f_i A_{th,i} \frac{N_i^+ (1 - P f_i A_{th,i}) - N_i^- (1 + P f_i A_{th,i})}{(1 - P^2 f_i^2 A_{th,i}^2)} = 0 \quad (15)$$

$P f_i A_{th,i}$ is small,

$$\frac{1}{1 - P^2 f_i^2 A_{th,i}^2} = 1 + 2P f_i A_{th,i} + \mathcal{O}(P^2 f_i^2 A_{th,i}^2) \quad (16)$$

Finally, neglecting all second-order terms,

$$P = \frac{\sum_{i=0}^{N_{bins}} f_i A_{th,i} (N_i^+ - N_i^-)}{\sum_{i=0}^{N_{bins}} f_i^2 A_{th,i}^2 (N_i^+ + N_i^-)} \quad (17)$$

To estimate the error on P , one needs to ensure that, in the final measurement, all yields are normalized by the accumulated charge measured for each helicity state. Each N_i^\pm is, in fact, a raw count n_i^\pm , normalized by FC^\pm (the charge measured by the Faraday Cup for each state \pm). Considering $\delta n_i^\pm = \sqrt{n_i^\pm}$, and propagating uncertainties assuming independence from all n_i^\pm , and neglecting second-order terms in $P f_i A_{th,i}$ once again,

$$\Delta P^2 = \frac{\sum_{i=0}^{N_{bins}} (f_i A_{th,i})^2 \left(\frac{N_i^+}{FC^+} + \frac{N_i^-}{FC^-} \right)}{\left(\sum_{i=0}^{N_{bins}} (f_i A_{th,i})^2 (N_i^+ + N_i^-) \right)^2}. \quad (18)$$

It is added in quadrature to the error coming from the dilution factor measurement (neglecting high-order terms once again):

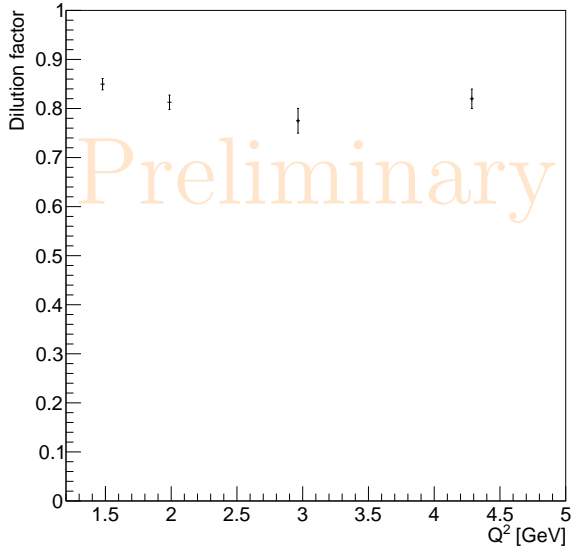
$$\Delta P_{f_i}^2 = \frac{\sum_{i=0}^{N_{bins}} A_{th,i}^2 (N_i^+ - N_i^-) \Delta f_i^2}{\left(\sum_{i=0}^{N_{bins}} (f_i A_{th,i})^2 (N_i^+ + N_i^-) \right)^2} \quad (19)$$

3.2 Dilution Factor

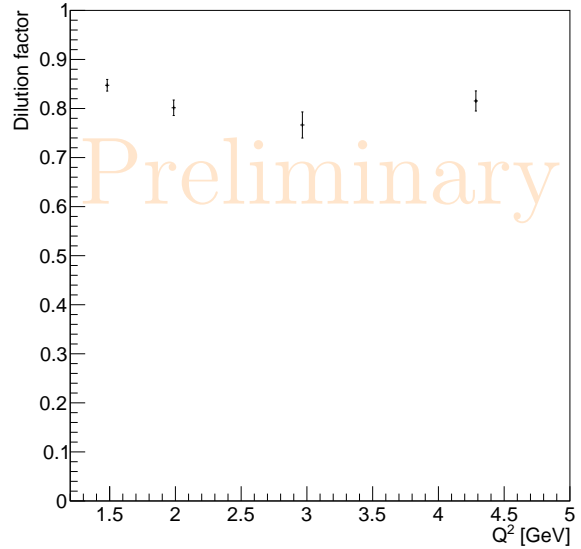
The dilution factor is estimated in bins of Q^2 as:

$$f_i = 1 - \frac{C_i}{NH_{3i}} \quad (20)$$

where C_i and NH_{3i} are yields after exclusivity cuts using C and NH_3 data. They are normalized to one another using the number of triggers recorded for each dataset since the FCup information is not available for part of the selected C runs. The dilution factor results are presented in Fig. 4 for the positively and negatively polarized datasets. The two datasets have compatible dilution factors within uncertainties.



(a) NH_{3-} runs



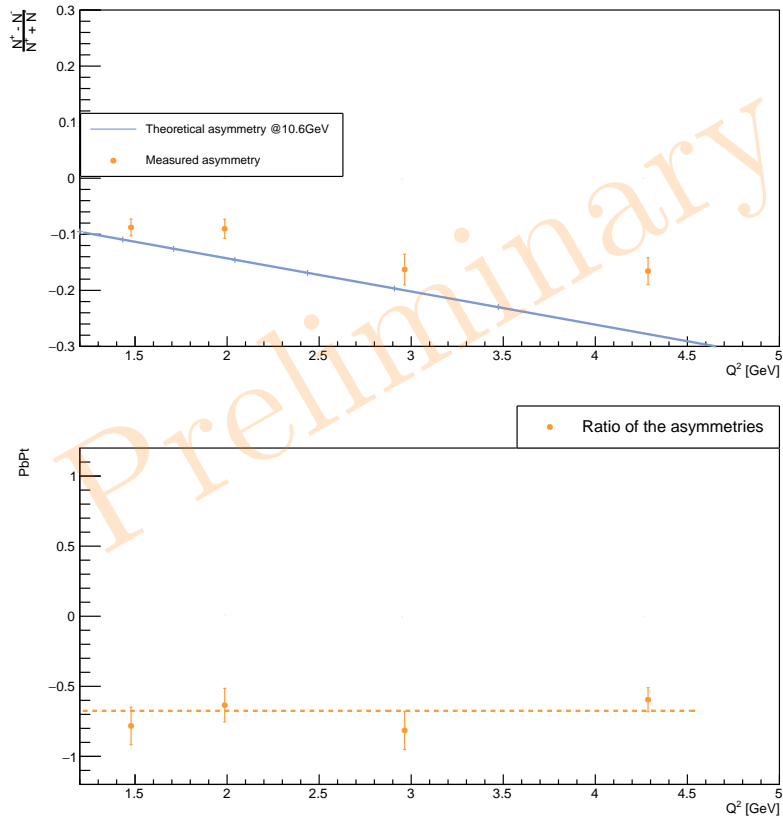
(b) NH_{3+} runs

Figure 4: Dilution factors from the elastic analysis. The left and right plot are for, respectively, negatively and positively polarized runs.

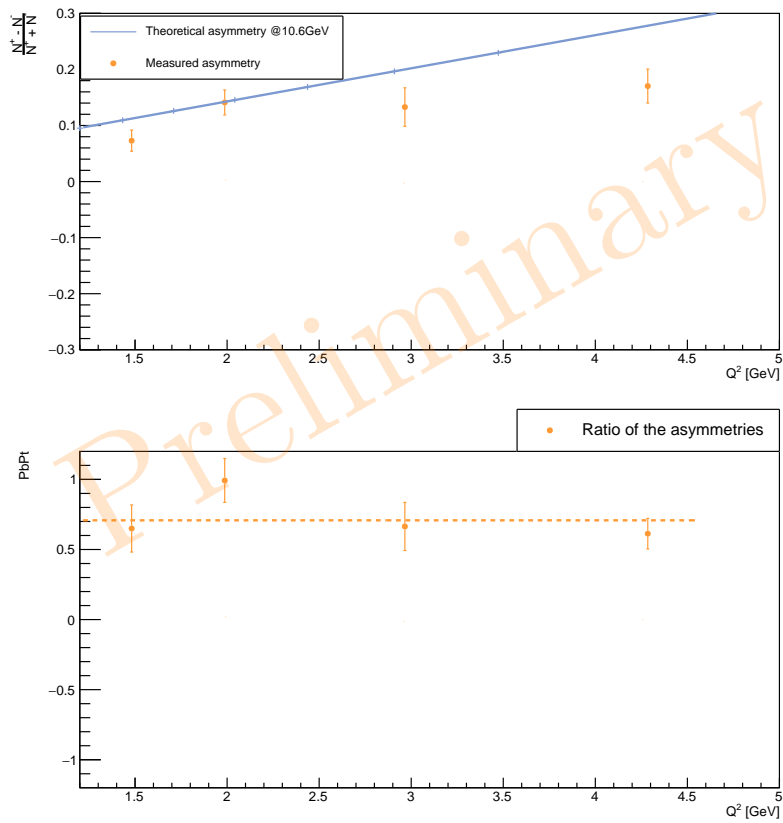
3.3 Results

Measurements of the polarization are finally presented in Fig. 5. The top plots show the theoretical and measured asymmetries in Q^2 bins. The bottom plots show the ratio of the two and their mean (dashed line) as an indication, but the final measurement is computed according to (17). The Q^2 dependence is mostly flat within uncertainty as expected, except for the second bin in the positively polarized dataset. The extracted values are:

- NH_{3+} : $P_b \times P_t = 0.692 \pm 0.085$
- NH_{3-} : $P_b \times P_t = -0.664 \pm 0.056$



(a) NH_3^- runs



(b) NH_3^+ runs

Figure 5: Elastic double spin asymmetry and target polarization.

4 DVCS analysis

4.1 Event Selection

Events with at least one proton, one electron, and one photon are selected from the "sidisdvcs" train which includes the following preliminary selections: $Q^2 > 0.95$ and $W > 1.95$ (both are computed from the electron kinematics using a beam energy of 10.5473 GeV as indicated by RCDB for the considered run range), the electron momentum needs to be above 1 GeV, and there is a cut on the vertex z position $-25 < v_z < 20$. From these events, all possible combinations of the final-state $ep\gamma$ are constructed.

A few preliminary cuts are added and are listed below.

- $Q^2 \geq 1 \text{ GeV}^2$
- $W \geq 2 \text{ GeV}^2$
- $E_\gamma \geq 1.5 \text{ GeV}$
- $\theta_{\gamma e} > 6.5^\circ$
- $MM_{eX\gamma}^2 < 5 \text{ GeV}^2$
- $\Delta t < 2 \text{ GeV}^2$
- $|MM_{ep\gamma}^2| < 0.4 \text{ GeV}^2$

First, tighter "DIS" cuts are applied to ensure we select events in a region where the GPD formalism can be applied. We also apply a cut on the photon energy since DVCS photons are expected to have relatively high energy. A cut on the angle between the reconstructed electron and photon is applied to remove clusters that have not been reconstructed properly in the FD (see Fig. 6). Finally, very loose cuts on missing masses and other exclusivity variables are applied to clean the sample.

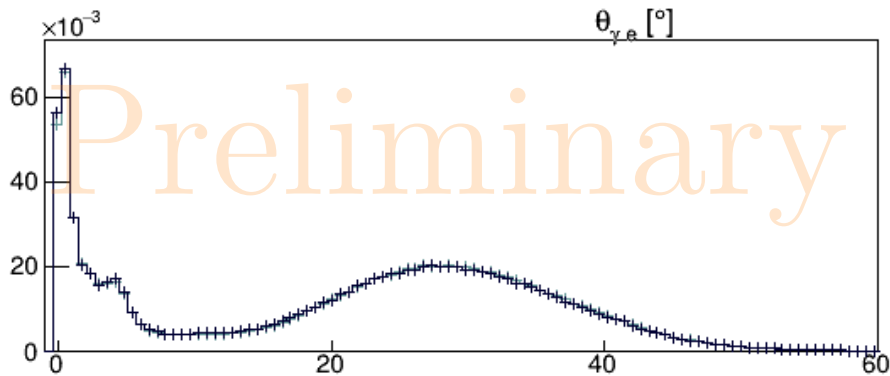
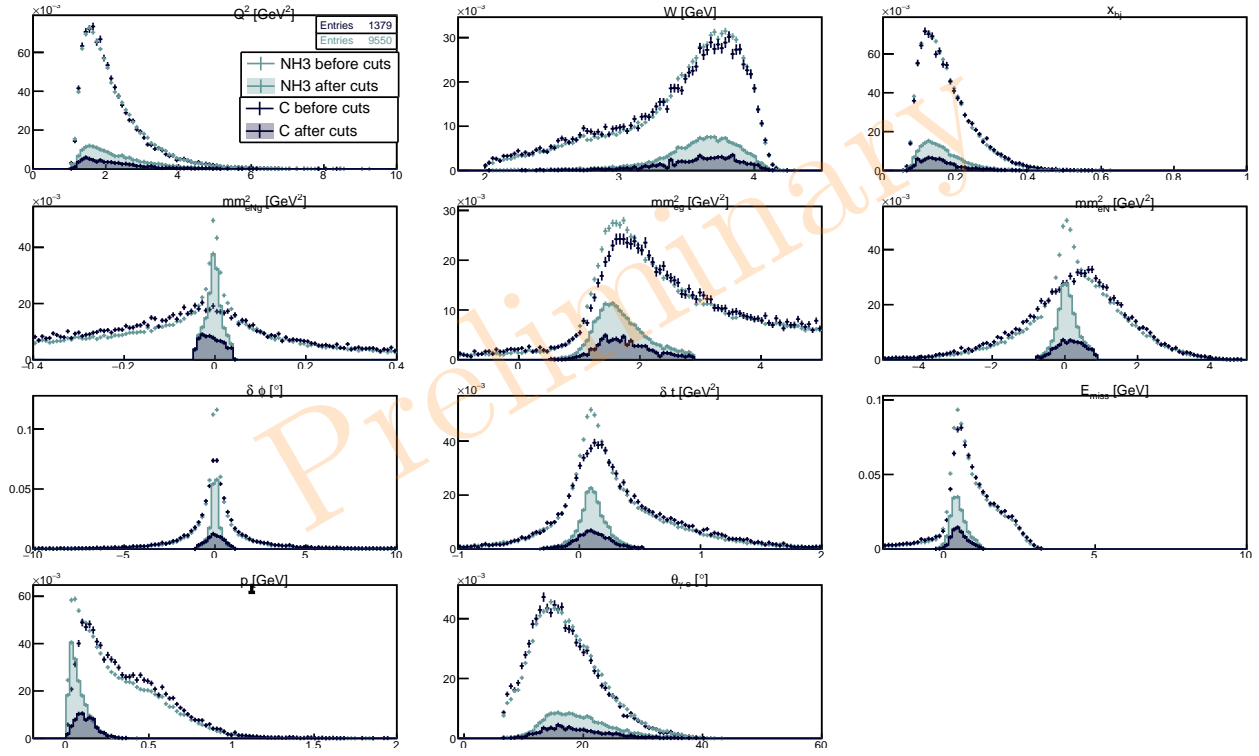


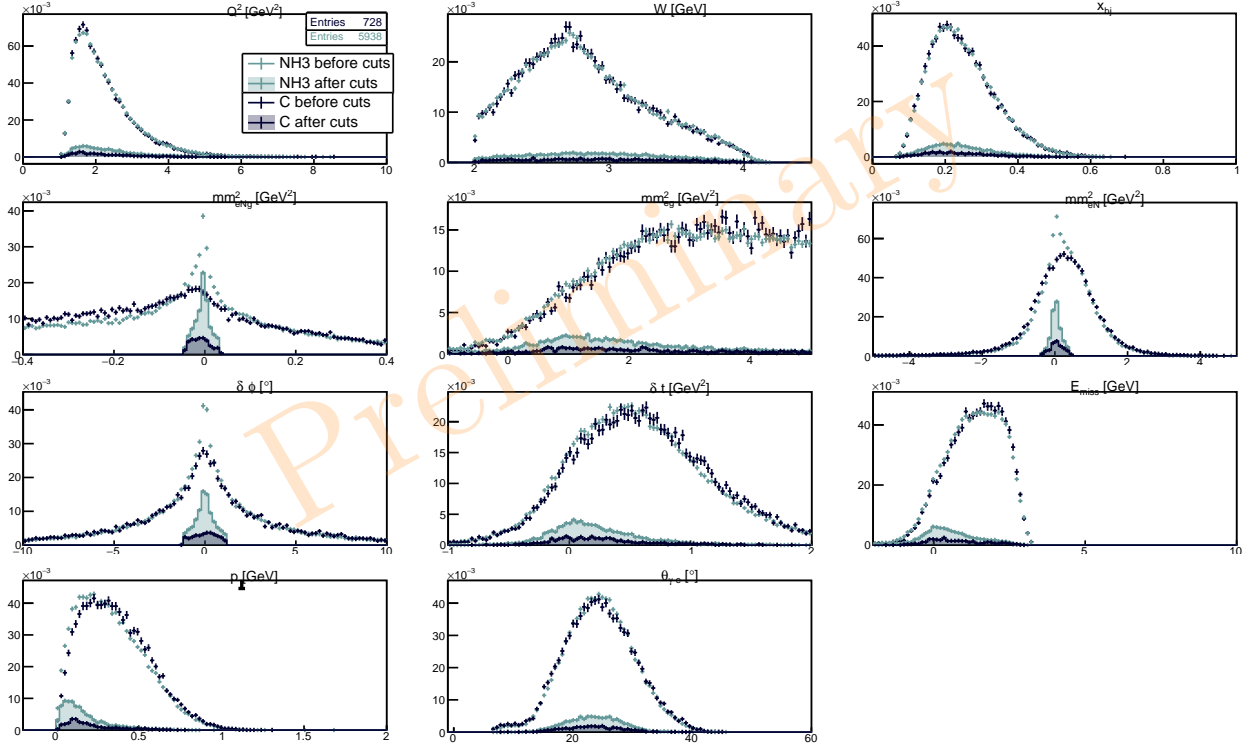
Figure 6: $\theta_{\gamma e}$ distribution for DVCS events with a photon in the FD. The low angle peak comes from clusters where part of the electron energy was not associated with it and was reconstructed as low-energy photons instead. A cut at 6.5° is applied to avoid these events.

Exclusivity cuts are then derived as 3σ cuts around the mean of Gaussian fits of the distributions of the exclusivity variables. They are derived separately for each topology of events, depending on where the particles were detected, and are shown in Fig. 7. Topologies not displayed are topologies where the H peaks could not be seen. For each plot, C data and NH_3 data are compared. The second line shows the missing masses of the $ep \rightarrow ep\gamma$, $ep \rightarrow e\gamma X$ and $ep \rightarrow epX$. $\delta\Phi$ is the difference between two ways of computing Φ . One uses the hadronic plane formed by the outgoing nucleon and virtual photon (computed from the kinematics of the incoming and outgoing electrons), and the other uses the hadronic plane formed by the outgoing photon and outgoing nucleon. δt is the difference between two ways of

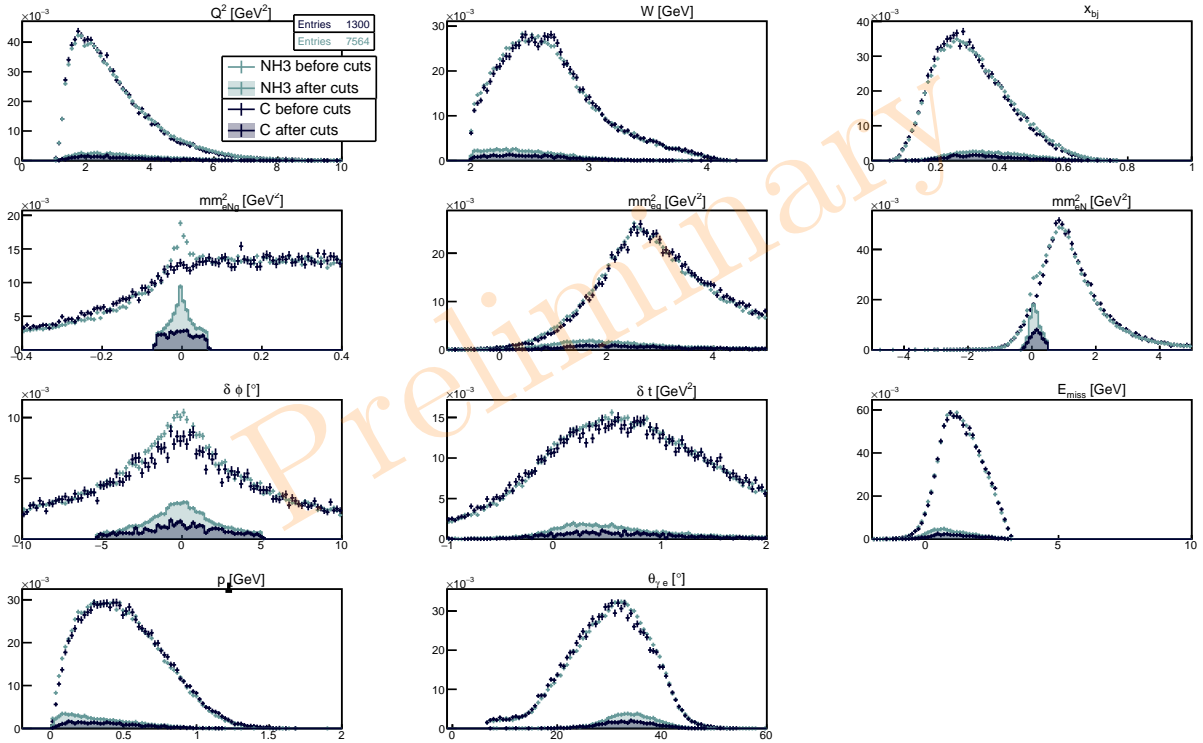
computing t , using $(p_p - p_{target})^2$ and $(p_{beam} - p_{e^-} - p_p)^2$. E_{miss} and p_{perp} are the missing energy and missing perpendicular momentum of the $ep \rightarrow ep\gamma$ system. $\theta_{\gamma e}$ is the angle between the electron and photon.



(a) FT photons, CD protons, FD electrons.



(b) FD photons, CD protons, FD electrons



(c) FD photons, FD protons, FD electrons

Figure 7: DVCS exclusivity variables for NH_3 (in green) and C (in black) data. The comparison before (simple points) and after (filled distribution) cuts highlights the selection of the H peak above the N background. The first row shows distributions for Q^2 , W and x_{bj} . The second row shows the missing masses of the $ep \rightarrow ep\gamma$, $ep \rightarrow eX\gamma$ and $ep \rightarrow epX$ systems. The third row shows the distributions of $\Delta\Phi$ and Δt which are differences in ways of computing Φ and t from the kinematics of the different final-state particles. It also shows the total missing energy of the $ep \rightarrow ep\gamma$ reaction. On the last row, p_{perp} is the total missing transverse momentum and $\theta_{\gamma e}$ is the angle between the final-state electron and photon.

After the exclusivity cuts, some candidates from the same events remain. However, they contribute to $< 0.1\%$ of the sample for the γ in “FTCDFD” (γ in the FT, p in the CD, e^- in the FD) topology, $< 0.2\%$ of the sample for the FDCDFD topology, and $< 0.6\%$ of the FDFDFD topology. Hence, they can be removed without a relevant loss of statistics.

4.2 Asymmetry Extraction

4.2.1 Dilution Factor

As with the elastic analysis, the dilution factor D_f is computed as the fraction of polarized events comparing NH_3 and C data similarly to Eq. (20).

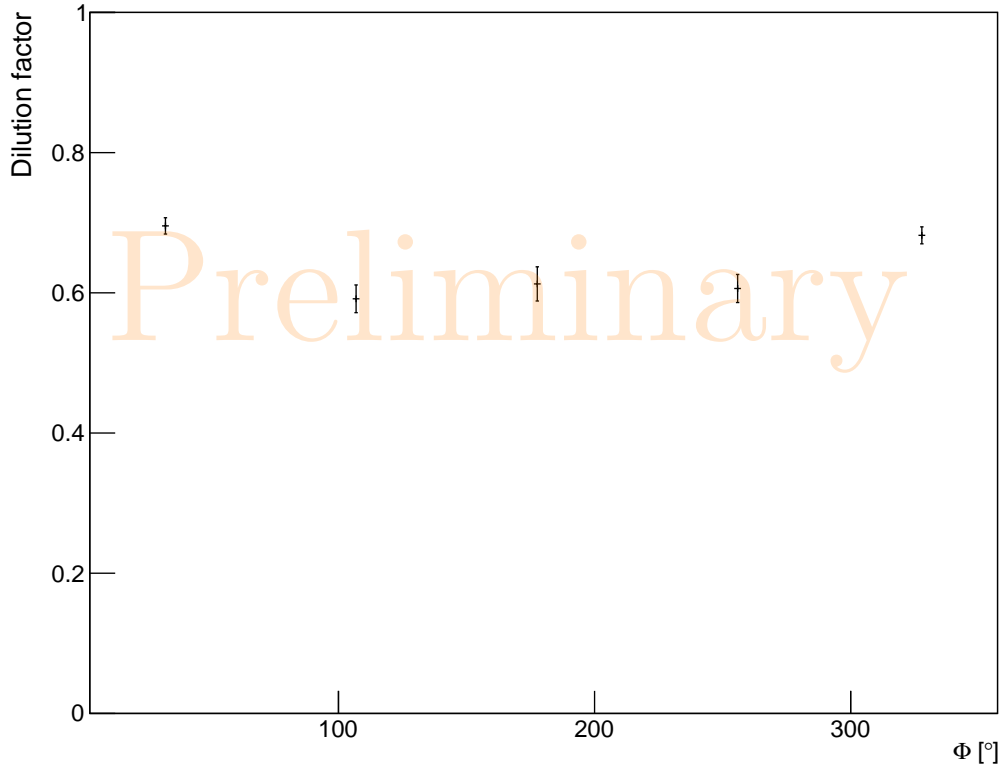


Figure 8: Dilution factor for the pDVCS events.

4.3 Asymmetries

The asymmetries are then computed in ϕ bins, according to:

- Beam-spin asymmetry

$$A_{LU} = \frac{P_t^-(N^{++} - N^{-+}) + P_t^+(N^{+-} - N^{--})}{Pb \times (P_t^-(N^{++} + N^{-+}) + P_t^+(N^{+-} + N^{--}))} \quad (21)$$

- Target-spin asymmetry

$$A_{UL} = \frac{N^{++} + N^{-+} - N^{+-} - N^{--}}{Df \times (P_t^-(N^{++} + N^{-+}) + P_t^+(N^{+-} + N^{--}))} \quad (22)$$

- Double-spin asymmetry

$$A_{LL} = \frac{N^{++} + N^{--} - N^{+-} - N^{-+}}{P_b \times Df \times (P_t^-(N^{++} + N^{-+}) + P_t^+(N^{+-} + N^{--}))} \quad (23)$$

where all yields are normalized by the appropriate Faraday Cup counts $N^{bt} = \frac{\text{yield}(b,t)}{\text{FCup counts}(b,t)}$. Results for the BSA, TSA, and TSA can be found in Fig.9,10, and 11, respectively. They are computed at the following central kinematics:

- $\langle Q^2 \rangle = 2.5 \text{ GeV}^2$
- $\langle x_{bj} \rangle = 0.2$
- $-t = 0.5 \text{ GeV}^2$

Results in blue do not use the FC information as normalization, while results in orange do. This normalization centers the asymmetries around zero as expected.

The amplitudes are delicate to comment on since these asymmetries are integrated over a vast range of kinematics and are still contaminated by π_0 production. The BSA, in particular, is lower than previous measurements for DVCS [2] since the N background is not accounted for. However, all asymmetries show the expected signs and shapes as sinusoidal functions of ϕ .

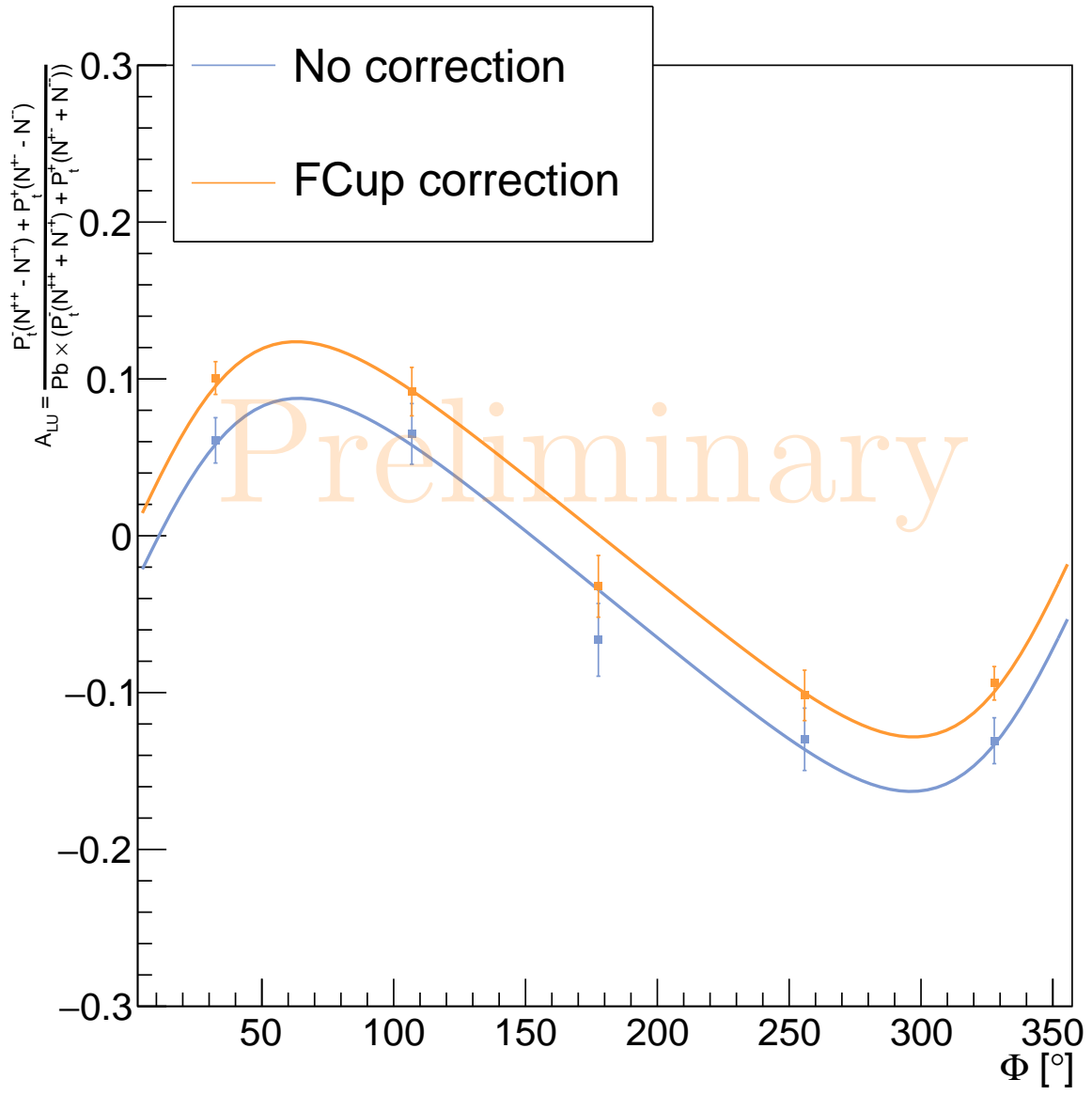


Figure 9: Preliminary beam spin asymmetry for pDVCS in NH_3 .

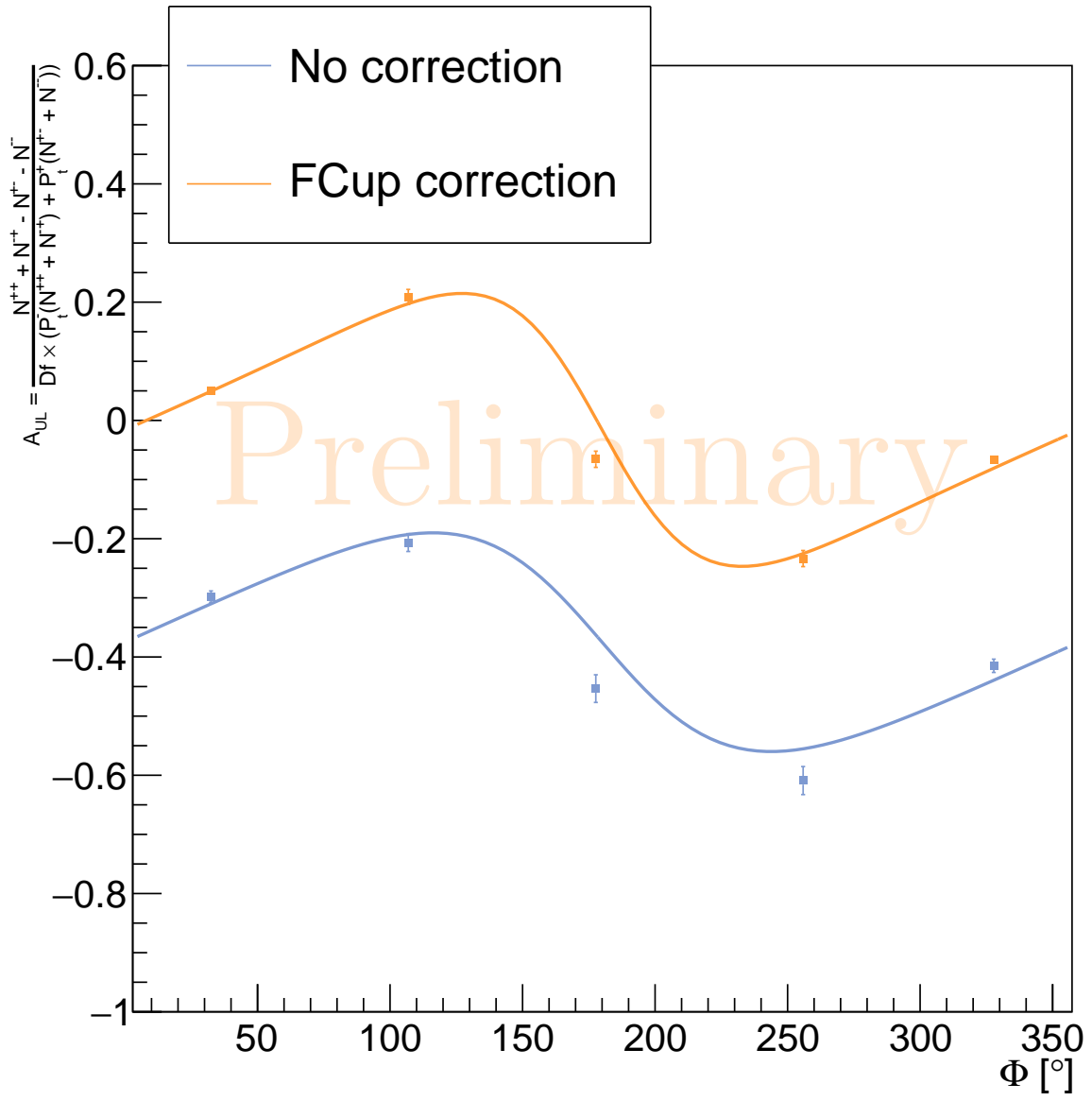


Figure 10: Preliminary target spin asymmetry for pDVCS in H .

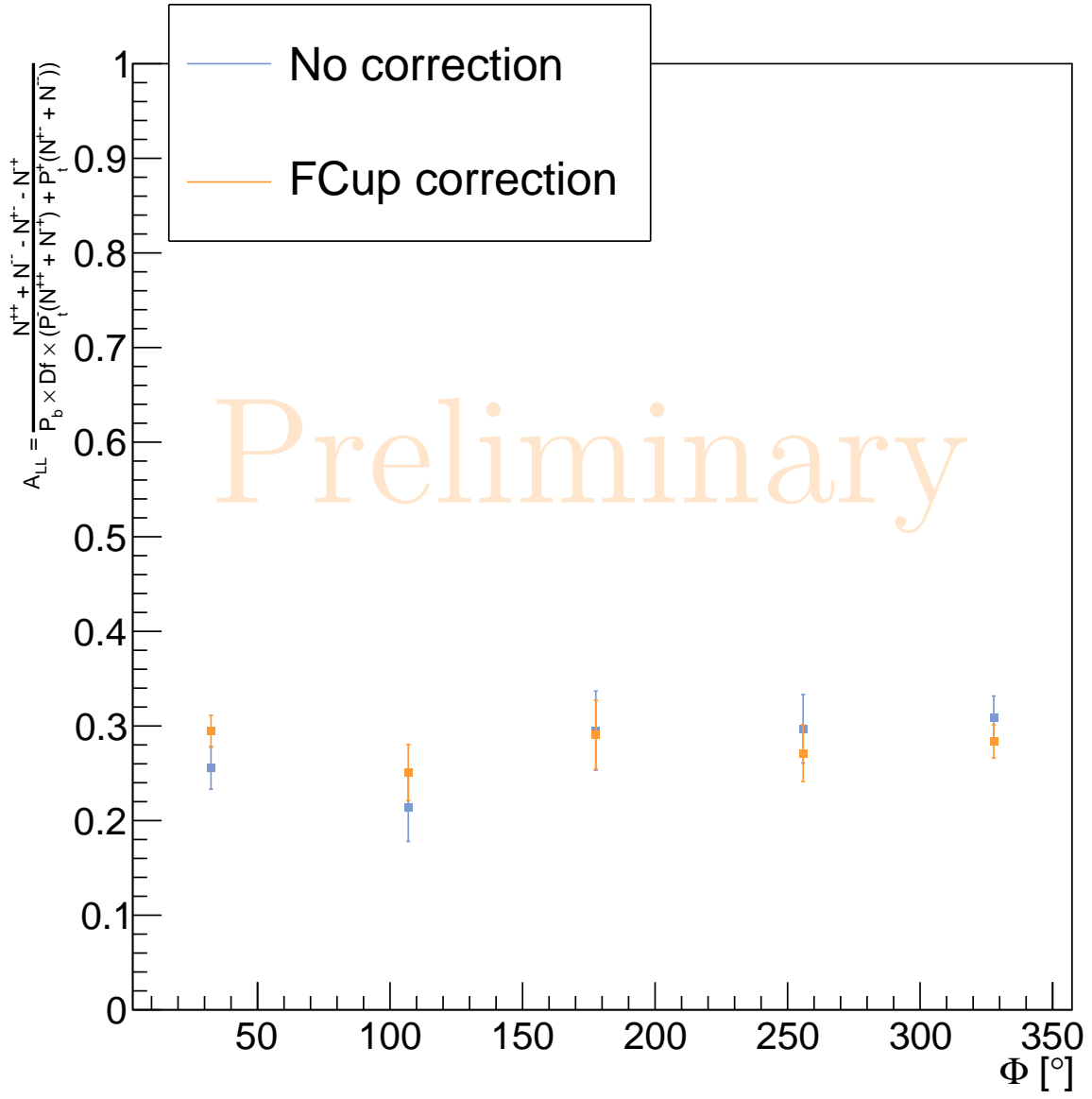


Figure 11: Preliminary double spin asymmetry for pDVCS in H .

References

- [1] J. Arrington. “Implications of the discrepancy between proton form factor measurements”. In: *Phys. Rev. C* 69 (2 Feb. 2004), p. 022201. DOI: 10.1103/PhysRevC.69.022201. URL: <https://link.aps.org/doi/10.1103/PhysRevC.69.022201>.
- [2] CLAS Collaboration G. Christiaens et al. *First CLAS12 measurement of DVCS beam-spin asymmetries in the extended valence region*. 2022. arXiv: 2211.11274 [hep-ex].